I

Publication I

W. Suttrop, V. Hynönen, T. Kurki-Suonio, P. T. Lang, M. Maraschek, R. Neu, A. Stäbler, G. D. Conway, S. Hacquin, M. Kempenaars, P. J. Lomas, M. F. F. Nave, R. A. Pitts, K.-D. Zastrow, the ASDEX Upgrade team, and contributors to the JET-EFDA workprogramme (2005). Studies of the "Quiescent H-mode" regime in ASDEX Upgrade and JET. *Nuclear Fusion*[†] **45**(7) 721–730.

[†] http://www.iop.org/journals/NF

INSTITUTE OF PHYSICS PUBLISHING and INTERNATIONAL ATOMIC ENERGY AGENCY NUCLEAR FUSION

Nucl. Fusion **45** (2005) 721–730 doi:10.1088/0029-5515/45/7/021

Studies of the 'Quiescent H-mode' regime in ASDEX Upgrade and JET

W. Suttrop[1], V. Hynönen[2], T. Kurki-Suonio[2], P.T. Lang[1], M. Maraschek[1], R. Neu[1], A. Stäbler[1], G.D. Conway[1], S. Hacquin[3], M. Kempenaars[4], P.J. Lomas[5], M.F.F. Nave[3], R.A. Pitts[6], K.-D. Zastrow[5], the ASDEX Upgrade team and contributors to the JET-EFDA workprogramme

[1] Max-Planck-Institut für Plasmaphysik, EURATOM Association, D-85748 Garching, Germany
[2] Euratom-TEKES Association, Helsinki University of Technology, PO Box 2200, FIN-02015 HUT, Finland
[3] Associação EURATOM/IST, Centro de Fusão Nuclear, Instituto Superior Técnico, 1049-001 Lisboa, Portugal
[4] FOM-Instituut for Plasmaphysica 'Rijnhuizen', Association EURATOM-FOM, PO Box 1207, 3430 Nieuwegein, The Netherlands
[5] Euratom/UKAEA Fusion Association, Culham Science Centre, Abingdon, Oxfordshire, OX14 3DB, UK
[6] Association Euratom-CRPP, Ecole Polytechnique Fédérale de Lausanne, 1015 Ecublens, Switzerland

E-mail: suttrop@ipp.mpg.de

Received 10 December 2004, accepted for publication 23 May 2005
Published 5 July 2005
Online at stacks.iop.org/NF/45/721

Abstract
The stationary edge localized mode (ELM)-free 'Quiescent H-mode' (QH-mode) regime, obtained with counter neutral beam injection, is studied in ASDEX Upgrade and Joint European Torus. QH-mode plasmas have high pedestal and core ion temperatures together with good High-confinement mode (H-mode). ELMs are replaced by continuous MHD oscillations, the 'edge harmonic oscillation' (EHO) and the 'high frequency oscillation'. Stationarity of particle and impurity densities is linked to the occurrence of these MHD modes. The EHO location in the steep-gradient region and its appearance with increasing edge pressure points towards the edge pressure or pressure gradient as possible drivers for the EHO. Injection of small cryogenic pellets can raise the plasma density to about 40% of the Greenwald density limit without triggering ELMs. Orbit following calculations of the slowing-down distribution show the presence of an enhanced fast particle density in the H-mode barrier region despite the large loss currents with counter-injection. The radial electrical field in the edge barrier region, about twice as large in QH-mode as in ELMy H-mode, is large enough to reverse the precession drift direction of injected beam ions, leading to a resonance of the EHO with the drift precession frequency.

PACS numbers: 52.55.Fa, 52.55.Tn

(Some figures in this article are in colour only in the electronic version)

1. Introduction

The 'High-confinement' mode (H-mode) is considered a reliable regime for achieving adequate fusion yield in the planned ITER experiment and in a nuclear fusion reactor. However, with large temperature and pressure values on top of the edge transport barrier (the H-mode 'pedestal'), type I edge localized modes (ELMs) are usually obtained. If the ablation thresholds for both metal and graphite divertors are exceeded [1], type I ELMs may impose unacceptable peak heat loads on the divertor target in a large-scale fusion device. Therefore, confinement regimes that allow for large pedestal pressure in order to maintain good confinement, but with small or no ELMs, are needed to prevent excessive erosion and migration of divertor material inside the tokamak vessel.

ELM-free H-modes are observed and are characteristic, for example, of the Hot ion H-mode [2] and VH-mode [3] improved confinement regimes. However, in both the regimes,

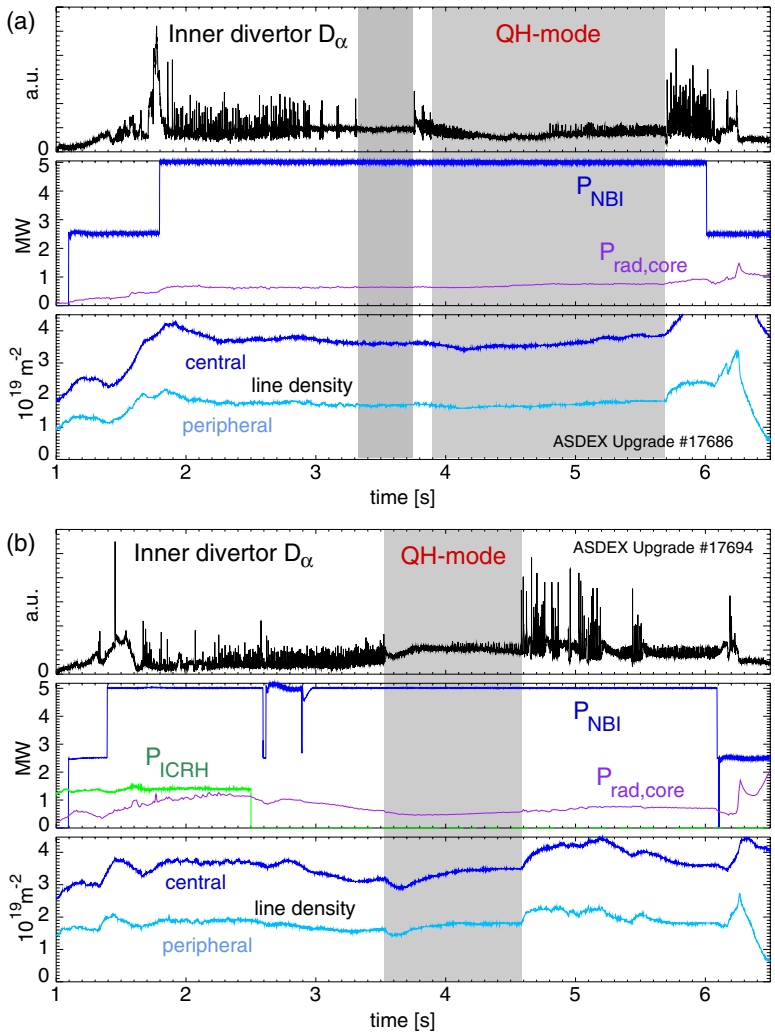

Figure 1. Time traces of QH-mode discharges in ASDEX Upgrade with (*a*) semi-tangential and (*b*) radial NBI sources. QH-mode phases are shaded in grey.

no stationary ELM-free phase can be maintained. Hot ion modes in Joint European Torus (JET) are characterized by a continuous increase in pedestal pressure until a large type I ELM occurs [4]. Particle transport analysis of ELM-free plasmas in DIII-D [5] suggests that the observed temporal evolution of the density is due to reduced diffusivity in the outer 20% of the minor radius.

The 'Quiescent' H-mode (QH-mode) regime, recently discovered in DIII-D [6] is ELM-free, but with stationary density and impurity content. At the same time, the confinement is comparable to or better than in a typical type-I ELMy H-mode. The QH-mode regime has been reproduced and studied in ASDEX Upgrade [7]. Meanwhile, H-mode behaviour similar to that of a QH-mode has been found in JT-60U [8].

Here we report further studies of QH-mode properties in ASDEX Upgrade and experiments to scale up the QH-mode regime to larger plasmas in JET. The next two sections summarize the conditions and phenomenology of the QH-mode in both the machines. Subsequently, we describe the properties of the MHD behaviour that replaces ELMs in QH-mode and discuss the possible reasons for the suppression of ELMs in this regime.

2. Phenomenology of QH-mode in ASDEX Upgrade

So far in ASDEX Upgrade, QH-mode has been seen only with counter-current neutral beam injection (NBI) (counter-NBI). In agreement with the experience in DIII-D [6], large plasma-wall clearance (in ASDEX Upgrade a typically 8 cm gap in the main chamber), good pumping (using the lower divertor cryo-pump) and low neutral gas pressure appear helpful in obtaining long stationary QH-mode phases. The experiments have been carried out with a plasma current of $I_p = 1$ MA and a toroidal field B_t between 2.0 and 2.5 T ($q_{95} = 3.6 \ldots 4.5$).

Figure 1 shows time traces of two pulses that enter QH-mode: #17686 with a mixture of two semi-tangential NBI sources (one at $E = 60$ keV beam energy with tangency radius $R_{tan} = 0.93$ m and one at $E = 93$ keV with $R_{tan} = 0.84$ m), and #17694 with two radial sources ($E = 60$ keV with $R_{tan} = 0.53$ m). The plasma configuration and the total NBI heating power are identical. In both the pulses, no gas fuelling is employed during the H-mode phase. The transition to QH-mode occurs earlier and the QH-mode phases are longer with more tangential injection, in line with observations at DIII-D [9]. Note that with more tangential injection the plasma

density evolves very slowly during the QH-mode phase, while with radial injection both edge and core densities, after an initial drop, increase to levels above those in ELMy H-mode before the transition.

A transition to QH-mode is also obtained with the pair of tangential NBI sources installed at ASDEX Upgrade ($E = 93$ keV with $R_{tan} = 1.29$ m, on the high field side), but the density quickly drops below the minimum density to avoid the NBI shine-through. Note that while radial and semi-tangential sources produce trapped particles in a wide radial range, the tangential sources produce mostly passing particles inside the plasma, and a significant trapped particle fraction only near the H-mode pedestal. In ASDEX Upgrade, QH-mode has been obtained at various levels of effective ion charge Z_{eff}, the lowest value obtained so far being $Z_{eff} = 2.5$ [10]. ELMy and QH-mode phases with counter-injection show similar values of Z_{eff}.

3. QH-mode experiments in JET

In 2003, during the reversed plasma current campaign in JET, dedicated experiments were carried out to identify the QH-mode regime in plasmas of larger size. The configuration used (shown in the inset in figure 3) combines large wall clearance (15 cm outboard and inboard gaps) and good exhaust by positioning the strike points for optimum cryo-pumping in the Mark II SRP Gasbox divertor. Low recycling conditions are obtained by a combination of He glow discharge cleaning, followed by a lengthy period of cryo-pumping and beryllium evaporation in the main chamber. Discharges are heated with up to 14 MW of counter-current neutral beams. Different combinations of plasma current and magnetic field are used: 2.5 MA/2.7 T ($q_{95} = 3.3$), 1.7 MA/2.15 T ($q_{95} = 4.9$), 1.7 MA/2.25 T ($q_{95} = 4.3$) and 1.5 MA/2.2 T ($q_{95} = 4.7$).

In these discharges, extended ELM-free phases with up to 1.5 s duration are found. Figure 2 shows pulse 59611 ($I_p = 2.5$ MA, $B_t = 2.7$ T, $q_{95} = 3.3$) with type I ELMs until $t = 17.2$ s, followed by an ELM-free phase until 18.6 s. During the ELM-free time interval, radiated power (top panel) and electron density (third panel) remain stationary, indicating that the particle confinement time is not increasing drastically in the absence of ELMs. This behaviour is as expected for QH-mode and is in contrast to the increase in density and radiation usually found in traditional ELM-free phases. As is often seen in the smaller machines with counter-injection at low density, Z_{eff} is high, ranging between 4 and 5 in JET, independent of the presence of ELMs. Confinement is at or above the H98y scaling [11], and no deterioration during the ELM-free phase is seen. These stationary ELM-free phases are accompanied by the characteristic edge harmonic oscillation (EHO), which is observed both in magnetic measurements and in X-mode reflectometry measurements with cut-off layer in the H-mode barrier region. We therefore identify these phases as transitions to the QH-mode regime in JET. In addition, pronounced core MHD behaviour is observed in most of the discharges. While the cases with $q_{95} = 3.3$ have sawteeth, the plasmas at higher q ($q_{95} \geqslant 4$) generally show $n = 1$ and $m = 1$ fishbone activity.

In figure 3, core temperature and density profiles of an ELMy and a QH-mode phase are compared in the same discharge. The electron cyclotron emission (ECE) and charge

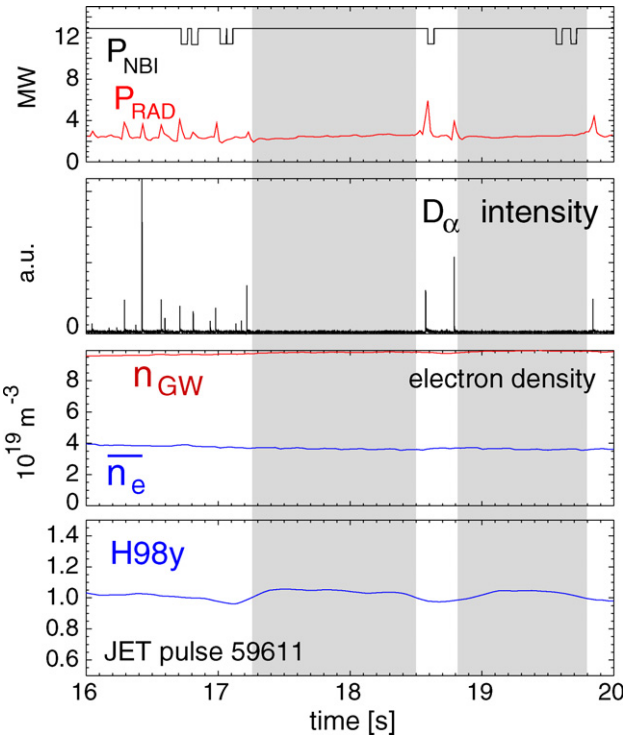

Figure 2. Time traces of JET pulse 59611 with an extended QH-mode phase (grey shaded).

exchange spectroscopy measurements (edge and core systems) indicate that there is little difference in electron and ion temperatures through most of the profile as well as at the H-mode pedestal top. Also, as shown by core LIDAR measurements, the plasma density is similar in the two regimes.

Although the observed ELM-free phases show many of the features characteristic of the QH regime, it has not been possible in JET to reproduce the same behaviour in repetitive pulses with identical parameters or to produce extended QH-mode periods for longer than about 1.5 s or three confinement times. It appears that the longest quiescent phases occur in plasmas produced immediately after the wall conditioning cycles or following repeated low recycling discharges with high NBI power and minimum external gas input.

4. MHD activity in QH-mode

QH-mode pulses usually show rich MHD activity. In the plasma core, fishbone or continuous $m = 1, n = 1$ oscillations prevail at higher edge safety factor, whereas at low q, sawtooth oscillations occur. A range of discharges has no discernible $m = 1, n = 1$ activity.

4.1. The edge harmonic oscillation

The most pronounced MHD feature of the QH-mode is that ELMs are replaced by the characteristic EHO [6]. The name originates from the many harmonics observed in spectrograms of magnetic measurements. In ASDEX Upgrade and JET, the EHO fundamental has so far always been found at a toroidal mode number $n = 1$. ECE and radially deconvoluted soft

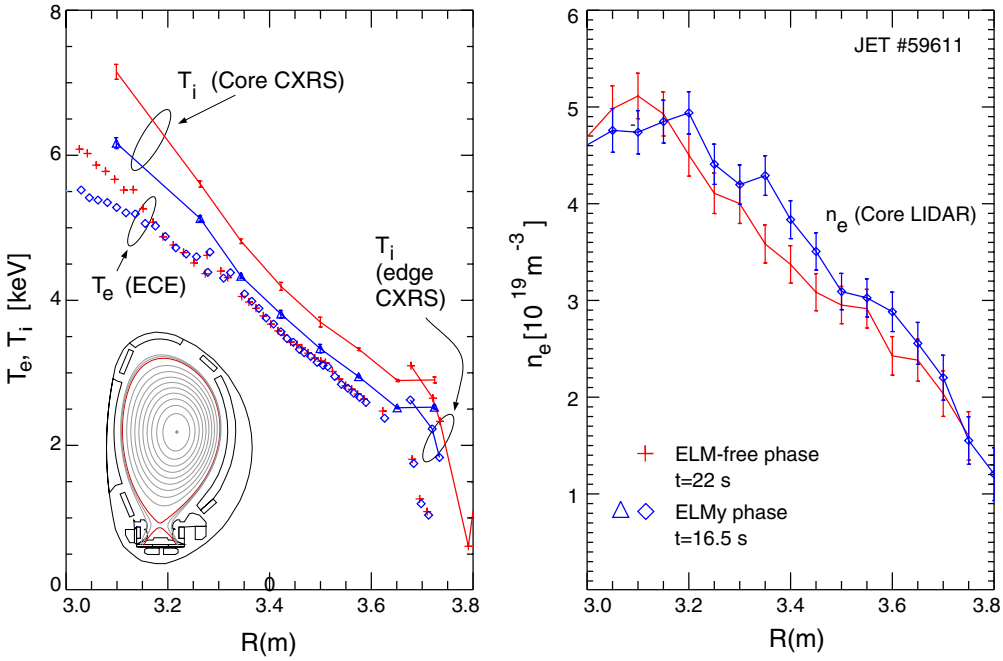

Figure 3. Temperature and density profiles in ELMy and QH phases of JET pulse 59611.

x-ray measurements in ASDEX Upgrade as well as microwave reflectometer data in JET show that the EHO is located in the H-mode edge transport barrier region.

Figure 4 (bottom trace) shows a spectrogram measured with the JET X-mode reflectometer [12,13] during a quiescent phase in JET pulse 59611. The probing frequency of 76 GHz corresponds to a cut-off position in the gradient region. The double-sided frequency spectrum from heterodyne detection (in phase and quadrature signals) shows an oscillation with a fundamental frequency of about 15 kHz and up to six harmonics (bright colours correspond to high intensity). The spectrum is symmetric, as expected for the radial launching direction of the reflectometer antennae. The middle trace represents the total intensity of the reflectometer signal, which varies little during the quiescent phase. There are fluctuations of the D_α intensity (top trace), which are correlated with the EHO frequency as seen in the reflectometer. For instance, in the time interval from $t = 22.05$ to 22.07 s the D_α intensity increases by about 50% while the EHO fundamental frequency drops from 15 kHz to about 11 kHz (the frequencies of its harmonics drop accordingly). This change is not due to a reduction of edge toroidal rotation velocity, as indicated by the charge exchange measurements of C^{6+}.

A safety factor scan in ASDEX Upgrade shows that the poloidal mode number adjusts itself such that the EHO remains localized on a flux surface in the gradient region [10]. The ECE measurement also reveals that the perturbations outside and inside the rational surface are in phase, as would be expected for a kink mode, and not in the case of a magnetic island.

Magnetic measurements at different toroidal locations show practically identical waveforms, the phase shifted according to the toroidal angle of the measurement as expected for an $n = 1$ mode. This suggests that the EHO is a rigidly rotating mode, i.e. the harmonic spectrum originates from its spatial structure, not from a time-dependent perturbation in the rotating frame.

Figure 5 shows the EHO waveform as seen by a radial field pick-up coil in ASDEX Upgrade (measuring $\mathrm{d}B_r/\mathrm{d}t$), which is located 10 cm from the separatrix at the outer midplane (upper trace). The raw signal is smoothed by a comb filter set to pass the EHO fundamental and its harmonics and reject noise at other frequencies. The filtered signal is integrated, resulting in a signal proportional to B_r (middle trace). The EHO fundamental frequency (here: 6.6 kHz) is found to vary in ASDEX Upgrade approximately between 6 and 12 kHz. For a kink-like perturbation the radial field B_r is proportional to the spatial derivative $\mathrm{d}\xi/\mathrm{d}l$ along a field line. Thus, for a rotating mode, the time integral of B_r gives a signal which is proportional to ξ as a function of toroidal angle. This signal is shown in the bottom trace. The sharp minima and maxima of the raw magnetic signal, which gives rise to the pronounced harmonic spectrum of the EHO, correspond to regions of large curvature near the minima and maxima of ξ. The EHO waveform can be described as near triangular.

4.2. *The 'high frequency oscillation'*

In addition to the EHO, an MHD oscillation at high frequencies occurs in ASDEX Upgrade [7], typically between 300 and 450 kHz and with a toroidal mode number of $n = 5$. Often, an additional higher frequency signal (not at an integer multiple frequency) is observed. The high frequency oscillation (HFO) amplitude is modulated in time (seen as characteristic bursts) as shown in figure 6, which compares a high-pass filtered fast B_r signal (middle trace) with the EHO (taken here from a peripheral soft x-ray chord and a slow magnetic signal with bandpass filter at the EHO frequency and its harmonics). The HFO envelope, with a toroidal $n = 0$ structure, has the same frequency and a fixed phase relationship with the EHO cycles for each toroidal location.

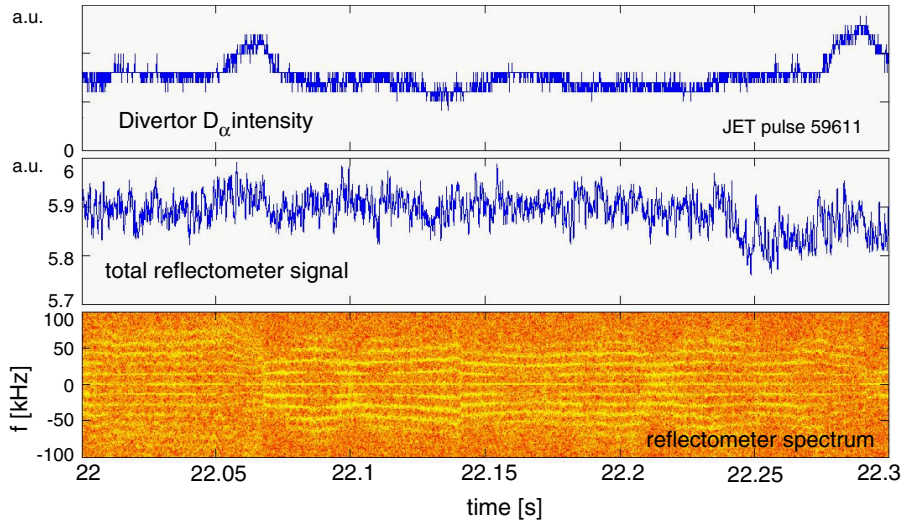

Figure 4. Observation of the EHO in JET with fixed frequency X-mode reflectometry: spectrogram (bottom trace), total reflected intensity (middle) and divertor D_α (top).

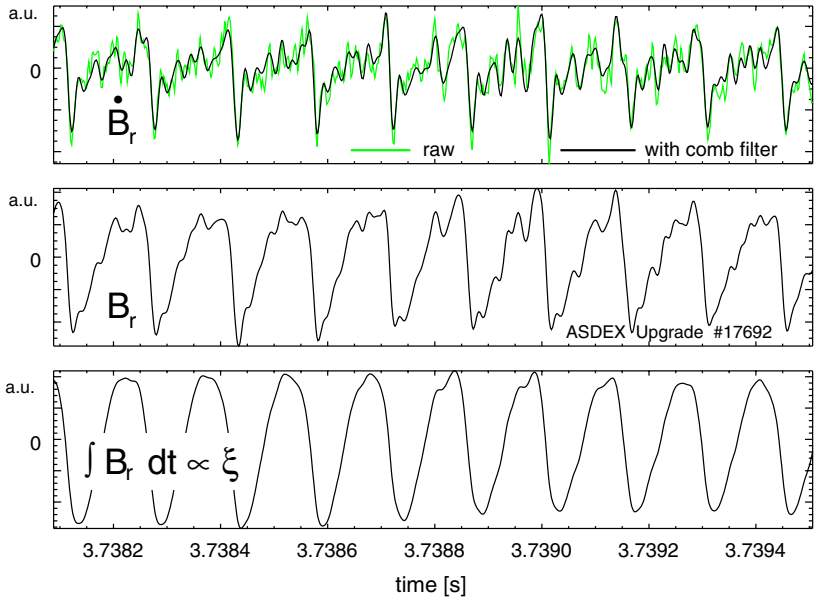

Figure 5. EHO signal of ASDEX Upgrade pulse 17692 measured by a magnetic probe (top), integrated once for B_r (middle) and integrated twice, yielding a signal proportional to the radial displacement ξ (bottom).

4.3. Transport associated with edge MHD activity

The absence of ELMs in H-mode usually causes a large increase in the particle confinement time, typically leading to an accumulation of deuterium and impurities. The H-mode phase is often terminated by an unusually large ELM or a thermal collapse of the plasma. In contrast, the density and radiation in QH-mode are quite stationary. One may ask whether the pronounced edge MHD causes or at least contributes to the particle and energy loss across the separatrix. Indeed, the HFO bursts and EHO cycles are strongly correlated with the outer divertor D_α intensity [7]. The inner divertor D_α signal shows no correlation. The D_α time lag of about 20 μs [7] is consistent with the transit time of ions at 10 keV energy to the divertor, i.e. typical of ions lost from the neutral beam slowing down distribution. If there are losses of thermal particles, they are overwhelmed by this signal.

Indirect evidence of thermal particle and heat losses associated with edge MHD in QH-mode comes from other observations. Figure 7 shows time traces of ASDEX Upgrade shot 18931, in which four pellets have been injected into a QH-mode plasma. The first three pellets result in a moderate but clearly visible increase in the core density. After the fourth pellet (at $t = 3.26$ s), the amplitude of the magnetic signal $\dot{B}_r$ drops and after this, the central and peripheral line densities are no longer stationary but continue to rise until several ELMs occur. Figure 8 shows a spectrogram of the magnetic signal that demonstrates the presence of the EHO before and in between pellet injection times and its disappearance after the last pellet is injected. We note that the disappearance of the EHO marks the loss of QH-mode and density control.

With counter-NBI, the EHO is often visible in ELMy phases as well, as shown in figure 9. The ELM times are

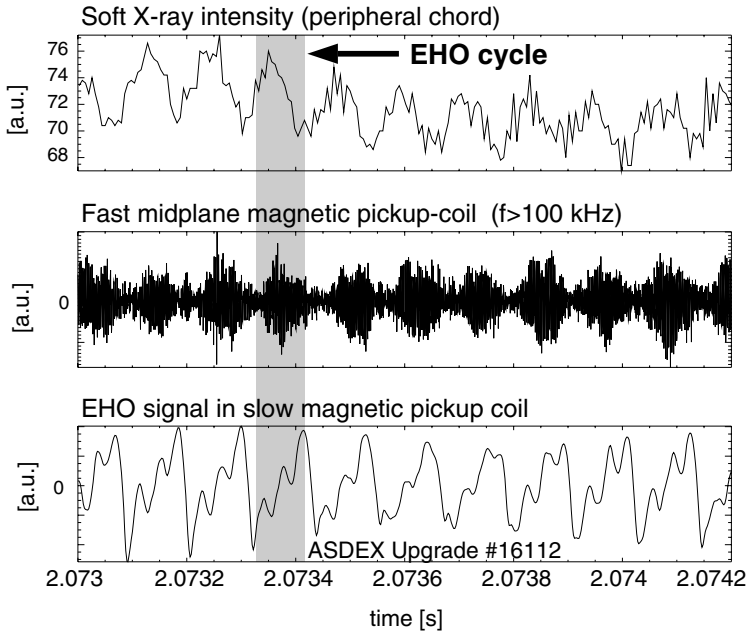

Figure 6. HFO (middle trace) and the temporal relation of HFO bursts with EHO cycles as seen in soft x-ray and magnetic measurements (above and below, respectively).

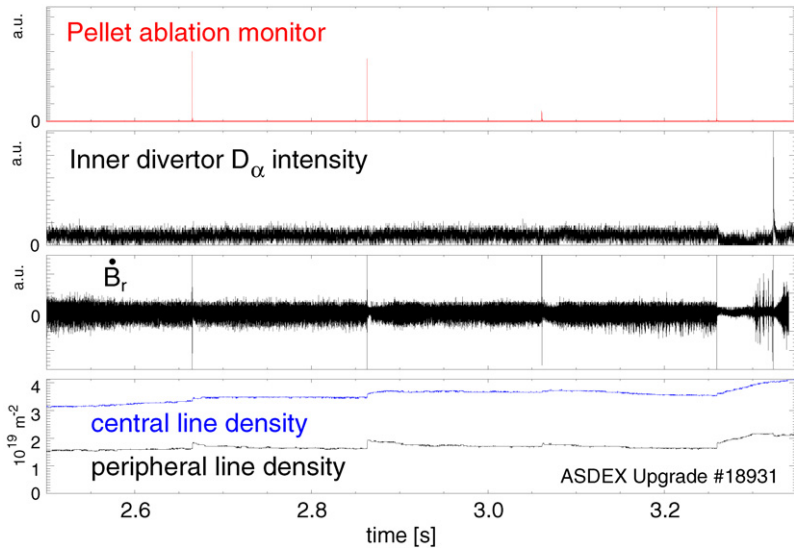

Figure 7. Pellet injection in QH-mode in ASDEX Upgrade: after the fourth pellet (at $t = 3.26$ s) the Mirnov coil amplitude decreases and the density begins to rise.

identified by the spikes in the divertor D_α signal. During the ELM cycle, the EHO (from measured $\dot{B}_r$ in between ELMs) appears only shortly before an ELM. The edge line density and pedestal top electron temperature (second panel) drop owing to the particle and energy losses associated with each ELM but recover rapidly within the first half of the inter-ELM cycle. Thereafter, they remain almost saturated until the next ELM occurs. The product of these signals is indicative of the pedestal top pressure, which shows the same temporal behaviour. The onset of the EHO in each cycle coincides with the beginning of the pressure saturation.

Since the heat flux from the plasma interior is continuous, this temporal behaviour suggests that with the onset of the EHO, heat transport across the edge barrier increases. In addition, the disappearance of the EHO after each ELM and its onset at the time the pressure recovers suggests that the pressure or edge pressure gradient in the barrier region plays a role in driving the EHO.

In order to study impurity transport across the H-mode barrier, silicon is injected into a QH-mode plasma by laser blow-off from a solid target (figure 10). The silicon content in the plasma core is monitored by a flat crystal Bragg spectrometer that measures the intensity of a Si XIII (He-like) line at a wavelength of 0.665 nm. The EHO is monitored by a radial field coil ($\dot{B}_r$). After the short injection pulse at $t = 2.59$ s, the EHO disappears and promptly, at $t = 2.65$ s,

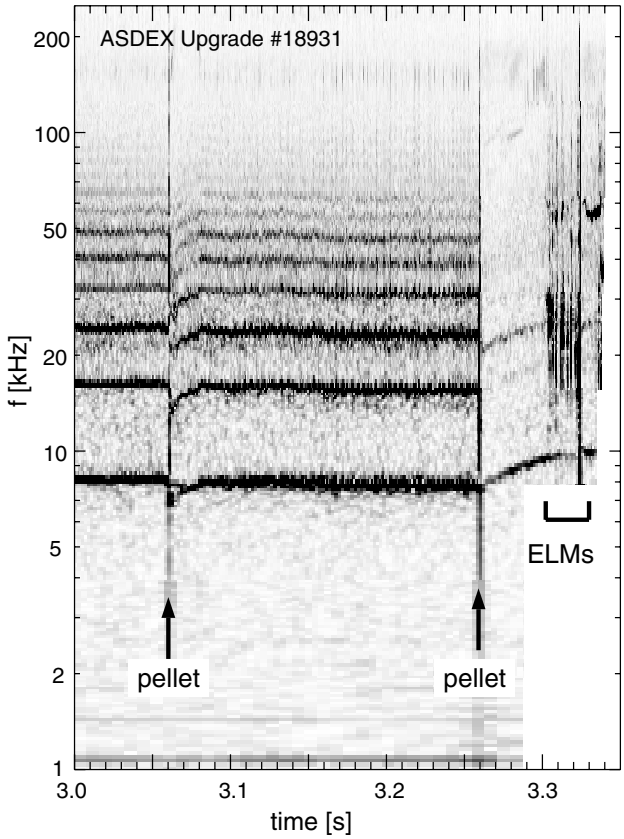

Figure 8. Spectrogram of the Mirnov coil signal showing the EHO and its disappearance after the last pellet of the shot shown in figure 7 at $t = 3.26$ s.

an ELM occurs. The EHO re-appears after this ELM and disappears again, followed by ELMs at 2.91 and 2.965 s. The Si XIII intensity drops during the first ELM and continues to decay during the EHO phases with a time constant of several hundred milliseconds. This time scale is similar to that determined in [14] for Si in ELMy H-mode plasmas with co-injection. We conclude that there is measurable impurity transport across the edge transport barrier whenever the EHO is present.

5. Fast particle effects

5.1. Fast particle distribution in the barrier region

In QH-mode, a strong enhancement (compared with ELMy H-mode) of the charge exchange neutral particle flux at high particle energies is observed [7]. This suggests a strong increase in the fast ion population at the plasma edge. The neutral beam slowing-down distribution is simulated using the Monte Carlo based particle following code ASCOT [15]. The magnetic equilibrium as well as the plasma temperature and density profiles are extracted from the ASDEX Upgrade QH-mode discharge #17695 at $t = 5.6$ s. Two NBI sources ($E = 60$ keV, $R_{\tan} = 0.93$ m) produce a flux of $\Gamma_{\mathrm{NBI}} = 7.3 \times 10^{20}$ particles s^{-1}. The ionization profiles for full, half and one-third energy components of the beam are calculated by the FAFNER code [16]. From the initial ion distribution (birth position, energy and pitch angle), a set of 10^5 test particles is generated, and the slowing-down is followed in ASCOT down to twice the thermal velocity. Orbits that intersect the limiter are counted as losses; the radial flux owing to these loss orbits is recorded as a function of radius. For counter-injection, the region for significant loss current is found to extend into the plasma down to a normalized poloidal flux radius $\rho_{\mathrm{p}} = 0.7$. The four-dimensional distribution function is recorded as the total time spent in slots of ρ_{p}, poloidal angle, total velocity v_{tot} and pitch $v_{\parallel}/v$. In a given phase space volume, the total number of actual plasma particles is the total time spent by test particles, multiplied by the ratio of particle source rate to the number of test particles. Thus, summing over all test particles during the simulation corresponds to steady-state injection. Figure 11 shows contour plots of a section of the fast particle distribution (time spent in seconds) as a function of radius ρ_{p} and total velocity v_{tot} for discharge #17695 (a), and for the corresponding co-injection case, obtained by reversing the initial pitch angles in the simulation (b).

For counter-injection (figure 11(a)), the maximum fast particle density extends further outward (to about $\rho_{\mathrm{p}} = 0.93$) than that for its co-injection counterpart ($\rho_{\mathrm{p}} = 0.85$, figure 11(b)). With the given beam geometry, almost all particles ionized near the H-mode pedestal top are trapped. Because of the outward-opening orbits in counter-injection there is a significant number of particles automatically aligned so that their orbits extend into the edge barrier region and, hence, to the resonant flux surface of the EHO. This population exists despite strong orbit losses from the plasma edge.

5.2. Reversal of the precession drift direction

For the magnetic field configuration used in the present counter-injection experiments, in the absence of a radial electrical field the toroidal drift precession is directed opposite to the injection direction. This is opposite to the observed rotation direction of the EHO and HFO, which rotate in the injection direction (the electron drift direction when projected to the plane perpendicular to the magnetic field).

However, a sufficiently large inward-directed radial electrical field E_r not only affects the magnitude of the precession drift frequency but can also reverse the direction of the precession drift. Experimentally, it is observed that the peak E_r in the H-mode barrier region for a fully established QH-mode is significantly larger than that for an ELMy H-mode. This is measured independently by Doppler reflectometry in ASDEX Upgrade [17], and, using radial force balance, from charge exchange spectroscopy in DIII-D [9]. A peak E_r of about -60 kV m^{-1} is found in ASDEX Upgrade QH-modes [17].

We consider the orbit of a typical ion representing the semi-tangential beam in ASDEX Upgrade. Such an ion is injected at an energy of 60 keV and has a pitch angle $v_{\parallel}/v$ of 0.45 at the outboard midplane. Figure 12 shows the effect of a homogeneous radial electrical field on the drift precession frequency of particles with $v_{\parallel}/v = 0.45$ born at different radii ρ_{p}, as calculated with ASCOT. In the absence of a radial electrical field the toroidal precession frequency ω_{prec} is about -60 to -70 krad s^{-1}. The critical radial electrical field for reversing the direction of the toroidal precession from counter-injection to co-injection is about -25 kV m^{-1}; more negative

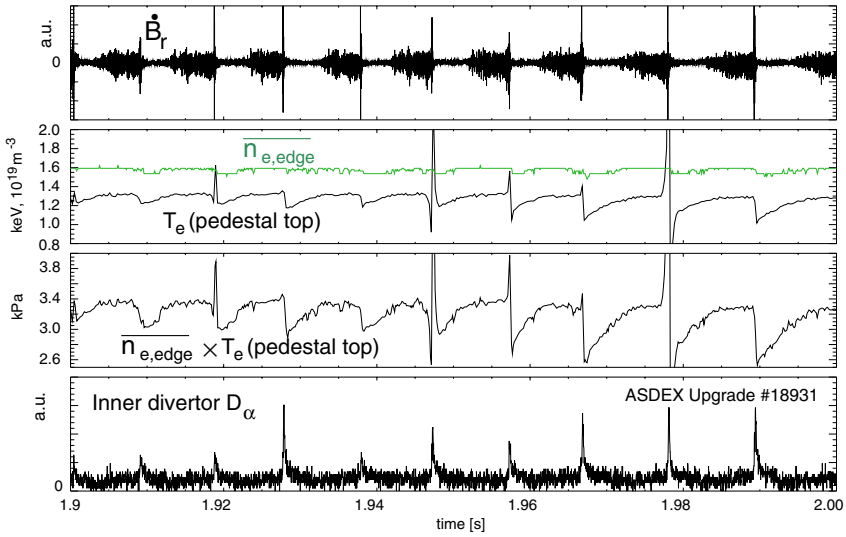

Figure 9. ELMy phase in a shot with counter-NBI. In between ELMs, the EHO appears as the pressure (approximated here as the product of edge line density and pedestal top electron temperature) approaches its maximum. With EHO present, the pressure saturates.

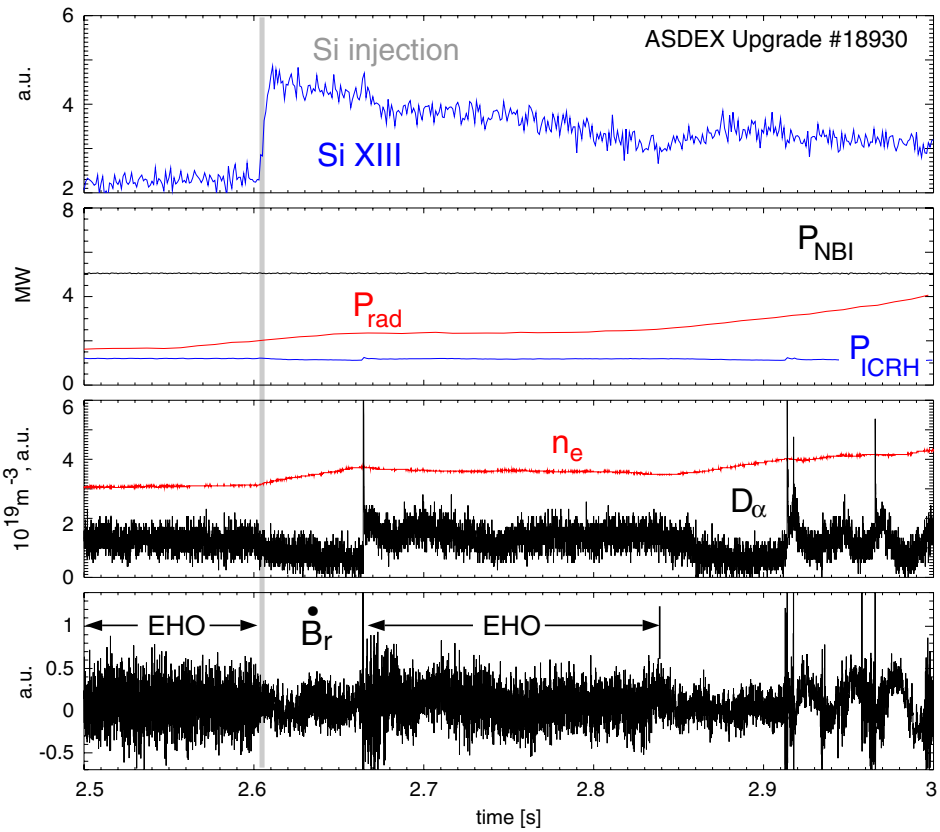

Figure 10. Impurity (Si) injection, monitored spectroscopically by Si XIII emission. The silicon content in the plasma continuously decreases after the injection. Phases during which the EHO occurs are marked.

values are observed in QH-mode in the pedestal region. Because of the shape of the q profile, ions born at smaller radii have higher positive precession frequencies. For $E_r = -60\,\mathrm{kV\,m^{-1}}$, a maximum of $\omega_{\mathrm{prec}} = 110\,\mathrm{krad\,s^{-1}}$ is reached. This frequency exceeds the rotation frequency of the EHO ($f = 7$–$11\,\mathrm{kHz}$, corresponding to $\omega_{\mathrm{EHO}} = 44$–$69\,\mathrm{krad\,s^{-1}}$). While the precession drift frequency is strongly affected by E_r, the bounce frequency changes very little (within about 10%).

We conclude that it is possible that a resonance between injected fast ions and the EHO occurs. The ASCOT calculations show that with counter-injection, the fast ion density in the edge barrier region is significantly larger than with co-injection because of the outward pointing ion orbits,

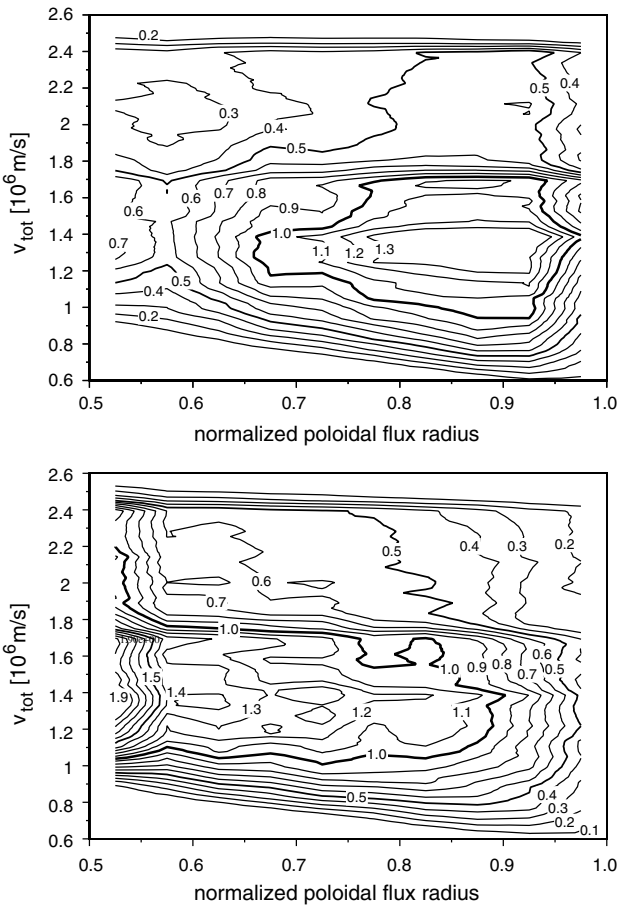

Figure 11. Fast ion population in the edge region as calculated by ASCOT (*a*) for ASDEX Upgrade shot #17695 at $t = 5.6$ s with counter-injection, (*b*) for identical plasma conditions but with co-injection.

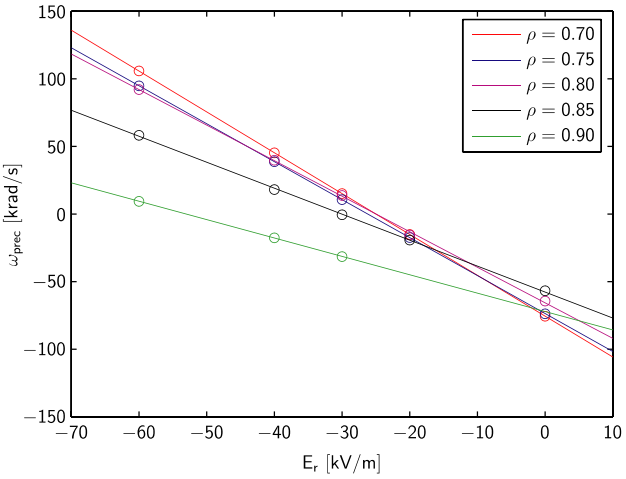

Figure 12. Effect of a spatially constant radial electrical field on the precession drift frequency (positive sign indicates co-injection direction) for different birth radii.

despite the increased orbit losses. Thus, it is possible that the fast ion population interacts with the EHO, a question that needs to be explored in further studies. An analogue observation of an edge MHD mode which is destabilized by

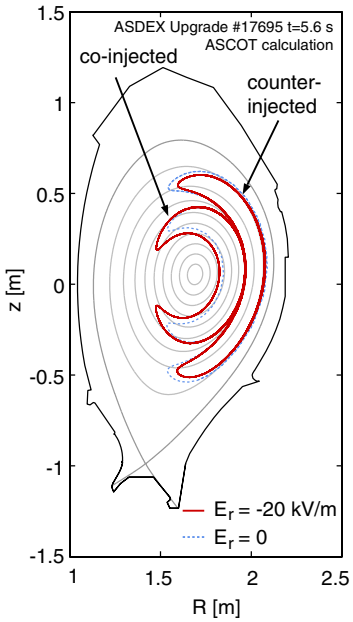

Figure 13. Orbits of co- and counter-injected ions born at $\rho_p = 0.7$ in the presence of a radially inward-directed electrical field of constant magnitude $E_r = -20$ keV (——) and $E_r = 0$ (- - - -).

fast particles might be the 'outer mode', a continuous $n = 1$ kink mode found in JET D–T discharges [18], which appears as the alpha particle population is slowly restored after giant ELM events.

5.3. Narrowing of ion orbits

A radial electrical field affects the width of fast particle orbits that intersect a region of significant E_r. With negative E_r, as is found in the H-mode barrier region, counter-injected trapped ions lose kinetic energy as they follow their drift orbits that take them radially outward. As a consequence, the radial width of their drift orbits is smaller than with zero or positive E_r. For co-injected particles, the orbits widen for $E_r < 0$ and shrink for $E_r > 0$. This effect of a radially inward-directed electrical field of constant magnitude is illustrated in figure 13, which shows the orbits of co-injected and counter-injected ions with 60 keV energy, born at $\rho_p = 0.7$, for $E_r = -20$ keV (solid lines), compared with the case $E_r = 0$ (dashed lines). This behaviour is analogous to the 'orbit squeezing' effect described in [19] for the case of an electrical field gradient.

The narrowing of the orbits also affects the fast particle density at the edge. For the experimental situation discussed earlier, and with $E_r = 0$, only ions born inside $\rho_p = 0.77$ have drift orbits that remain entirely inside the separatrix. A negative (inward-directed) E_r reduces the orbit width and, thus, increases the number of ions in the pedestal region. The experimentally observed E_r profile is modelled here with a simple square well for a semi-quantitative picture. With $E_r = -20\,\mathrm{kV\,m^{-1}}$ inside $\rho_p = 0.9$ and $E_r = -60\,\mathrm{kV\,m^{-1}}$ for $\rho_p = 0.9$–1.0, it is found that even ions born at $\rho_p = 0.81$ will remain inside the main plasma. Consequently, a higher fast ion density can build up in the H-mode barrier region in

the presence of a negative radial electrical field such as that observed in QH-mode.

6. Summary and conclusion

The quiescent H-mode regime combines stationary good confinement, high pedestal pressure and low pedestal collisionality ($\nu^* < 1$) with the absence of ELMs. So far, QH-mode is obtained only with counter-NBI. Good pumping conditions achieved, e.g. by placing the strike points in a position for good divertor pumping, seem to facilitate access to QH-mode. However, it is not yet possible to quantify the access conditions for QH-mode. Longest QH-mode phases in ASDEX Upgrade (ELM-free for the entire heating phase) and JET (ELM-free for about 1.5 s) have been found after fresh vessel conditioning, but it is difficult to say whether the change in the recycling conditions or suppression of impurity influx is influencing the QH-mode access. High Z_{eff} is often found with counter-injection, but it is not necessarily an essential property of QH-mode. The impurity mix in QH-mode and ELMy phases with counter-NBI is quite similar and depends more on the machine conditions than on the presence or absence of ELMs. Edge transport in QH-mode seems to be linked with the occurrence of the EHO and the HFO, which are always seen in QH-mode phases, and sometimes also in between ELMs. So far, the EHO is observed only with counter-NBI in ASDEX Upgrade. It is also unclear whether QH-mode discharges can be fuelled up to densities closer to the Greenwald limit. Gas puffing usually leads to a rapid transition to ELMy H-mode. First experiments with pellet fuelling show that pellets do not trigger ELMs in a QH-mode as they usually do in ELMy H-modes with co-NBI [20]. So far, the density increase is limited to about 40% of the Greenwald density. The QH-mode density limit is marked by the disappearance of the EHO and a transition to a non-stationary phase terminated by ELMs.

The slowing-down population of beam-injected particles is modelled with the ASCOT Monte Carlo code to study the effect of counter-injection and large edge radial electrical field, both characteristic features of QH-mode. Outward-pointing particle orbits lead to larger ion losses and a fast particle density gradient, which is aligned to the steep density gradient region at the plasma edge. In the presence of a strong radial electrical field the width of the ion orbits is modified; for counter-injection the width decreases with a negative, i.e. inward-directed field. The large radial electrical field ($\max(\|E_r\|) \approx -60\,\mathrm{kV\,m^{-1}}$ in the barrier) leads to a reversal of the precession drift of those particles which spend a significant time during their orbits in the E_r region. Based on this simulation, for a fraction of the slowing-down particles, a resonance can occur with the EHO.

A related, interesting question is what causes the suppression of ELMs in QH-mode. The main observations are as follows:

1. The edge current and pedestal top pressure in the barrier are not reduced as compared with the ELMy H-mode. This is likely to be true of the current density and pressure gradient as well.
2. In fully established QH-mode, the E_r well in the edge barrier region is significantly deeper than in the ELMy H-mode.
3. A significant population of trapped high-energy particles exists at the plasma edge, self-aligned with the H-mode barrier region owing to ionization in the high-density core and extending into the edge because of the outward pointing drift orbits associated with counter-NBI.

The first observation implies that reaching the same edge pressure gradient and the same edge current density as just before ELMs is not sufficient to generate an ELM event. The latter two observations point at a possible suppression of ELMs, either by strong $E \times B$ velocity shear or by finite Larmor radius stabilization by fast particles. These possibilities require further experimental and theoretical investigation.

Acknowledgments

The authors would like to thank S Günter for valuable discussions and CSC, the Finnish IT centre for science, Espoo, Finland (`www.csc.fi`), for providing the resources to run the ASCOT code.

References

[1] Federici G. *et al* 2003 *J. Nucl. Mater.* **313–316** 11
[2] Nave M.F.F., Lomas P., Gowers C., Guo H., Hawkes N., Huysmans G.T.A., Jones T., Parail V.V., Rimini F., Schunke B. and Thomas P. 2000 *Plasma Phys. Control. Fusion* **42** A89
[3] Osborne T.H. *et al* 1994 *Plasma Phys. Control. Fusion* **36** A237
[4] Nave M.F.F. *et al* 1999 *Nucl. Fusion* **39** 1567
[5] Baker D.R., Wade M.R., Jackson G.L., Maingi R., Stockdale R.E., deGrassie J.S., Groebner R.J., Forest C.B., Porter G.D. and DIII-D Team 1998 *Nucl. Fusion* **38** 485
[6] Burrell K.H. *et al* 2002 *Plasma Phys. Control. Fusion* **44** A253
[7] Suttrop W. *et al* 2003 *Plasma Phys. Control. Fusion* **45** 1399
[8] Sakamoto Y., Shirai H., Fujita T., Ide S., Takizuka T., Oyama N. and Kamada Y. 2004 *Plasma Phys. Control. Fusion* **46** A299
[9] Burrell K.H. *et al* 2004 *Plasma Phys. Control. Fusion* **46** A165
[10] Suttrop W. *et al* 2004 *Plasma Phys. Control. Fusion* **46** A151
[11] ITER Physics Expert Groups on Confinement and Modelling and Transport and Confinement Modelling Database and ITER Physics Base Editors 1999 *Nucl. Fusion* **39** 2175
[12] Conway G.D., Vayakis G., Fessey J.A. and Bartlett D.V. 1999 *Rev. Sci. Instrum.* **70** 3921
[13] Hacquin S., Meneses L., Cupido L., Cruz N., Kokonchev L., Prentice R. and Gowers C. 2004 *Rev. Sci. Instrum.* **75** 3834
[14] Dux R., Neu R., Peeters A.G., Pereverzev G., Mück A., Ryter F., Stober J. and ASDEX Upgrade Team 2003 *Plasma Phys. Control. Fusion* **45** 1815
[15] Heikkinen J.A., Herrmann W. and Kurki-Suonio T. 1997 *Plasma Phys.* **4** 3655
[16] Lister G.G. 1985 *Technical Report* 4/222, IPP, Garching, Germany
[17] Conway G.D., Schirmer J., Klenge S., Suttrop W., Holzhauer E. and ASDEX Upgrade Team 2004 *Plasma Phys. Control. Fusion* **46** 951
[18] Cottrell G.A., Bhatnagar V.P., Da Costa O., Dendy R.O., Jacquinot J., McClements K.G., McCune D.C., Nave M.F.F., Smeulders P. and Start D.F.H. 1993 *Nucl. Fusion* **33** 1365
[19] Hazeltine R.D. 1989 *Phys. Fluids* B **1** 2031
[20] Lang P.T. *et al* 2004 *Nucl. Fusion* **44** 665